Journal of Materials Chemistry C

PAPER

View Article Online
View Journal | View Issue

Cite this: J. Mater. Chem. C, 2018, 6, 7232

Experimental and computational conductivity study of multilayer graphene in polypropylene nanocomposites†

Roxana M. del Castillo, [a] Luis F. del Castillo, [b] Alipio G. Calles[a] and Compañ Vicente *[c]

We study the electric conductivity of compounds formed by multilayer graphene in polypropylene. Our study makes a comparative analysis between the experimental and computational results. To obtain an experimental measurement of the electronic properties, we deposited multilayer graphene (MLG) nanoparticles over a polypropylene matrix. The deposition was made over several stages, in which we added to the polymer matrix different percentages of MLG nanoparticles using the melt compounding technique, and we studied the conductivities of the nanocomposites by means of electrochemical impedance spectroscopy (EIS). The second part consists of computational calculations, in which we studied the electronic properties of a graphene sheet under a polypropylene molecule with different slabs in the monomer. In both analyses, there is a strong percolation phenomenon with a percolation threshold of around 18% of the MLG nanoparticles. Before the percolation threshold, the charge carriers are constrained in the polypropylene molecule, making the system an insulating material and creating p-type doping. After the percolation threshold, the charge carriers are constrained in the graphene, making the system a conductor material and creating n-type doping with conductivity values of around 20 S m^{-1}. This phenomenon is a consequence of a change in the mechanism of charge transfer in the interface between the polypropylene molecule and graphene sheet. To describe the charge transfer mechanism, it is necessary to consider the quantum effect. The incorporation of the quantum effects and the percolation phenomenon make it possible for the theoretical conductivity to be close to the conductivity measured experimentally.

Received 8th March 2018,
Accepted 29th May 2018

DOI: 10.1039/c8tc01135d

rsc.li/materials-c

1. Introduction

Polypropylene is one of the most popular thermoplastic polymers due it having many industrial applications.[1] Propylene alone is an insulating material, but researchers have proven that polymers with a small number of nanoparticles as fillers show enhanced physical properties, like thermal or electrical conductivity,[2] soundproofing ability and certain mechanical properties.[3] The above characteristics ensure that the electrically conductive filler/polymer is an important emerging type of material. The electrically conductive filler/polymer has been shown to have unique physical properties, such as lightweight, high thermal and electrical conductivity and ease of manufacture. Also, this kind of material is promising for electromagnetic interference shielding,[4,5] the construction of bipolar plates of fuel cells,[6,7] and high-dielectric materials for charge storage.[8,9] Usually, the nanofillers chosen are nanoparticles with high conductivity, such as multiwalled carbon nanotubes,[10] graphene layers,[11–15] multilayer graphene,[10] carbon nanofibers, and exfoliated graphite nanoplatelets.[16]

Previous experiments with multiwall carbon nanotubes (MWCNTs)[10] and multilayer graphene (MLG) nanoparticles have been performed over a polypropylene matrix; microwave heating has been used to estimate the effects of the filler in the polymer matrix.[17,18] Carbon nanotubes are more susceptible to microwave radiation compared with graphene multilayers, proving that graphene multilayers could be a better filler than the carbon nanotubes.[19] There is a percolation threshold in the number of nanoparticles over which the physical behavior changes drastically; this threshold depends on the geometric parameter called the aspect ratio of the fillers.[20] It has been observed that the percolation threshold is small in comparison

[a] Departamento de Física, Facultad de Ciencias, Universidad Nacional Autónoma de México, Mexico City 04510, Mexico
[b] Departamento de Polímeros, Instituto de Investigaciones en Materiales, Universidad Nacional Autónoma de México, Apdo. Postal 70-360, Mexico City 04510, Mexico
[c] Departamento de Termodinámica Aplicada, Escuela Técnica Superior de Ingenieros Industriales (ETSII), Universidad Politécnica de Valencia, Campus de Vera s/n, 46020-Valencia, Spain. E-mail: vicommo@ter.upv.es

† Electronic supplementary information (ESI) available. See DOI: 10.1039/c8tc01135d

with the number of nanofillers introduced in polymer systems. The percolation phenomenon has been seen from the experimental point of view and theoretically described with the Monte Carlo method. The classical point of view has predominated[21–23] in the description of the percolation, but we think that it is necessary to consider the quantum effects to represent the interface correctly. In the classical description of the percolation, it is usually assumed that the small percolation threshold of the graphene nanoparticles over a polymer matrix is a direct consequence of the hopping of the charge carriers,[24] but there is much more to study.

In this work, we are studying the electrical conductivity from an experimental and a theoretical point of view. For the experimental point of view, percentages of 0.5%, 1%, 3%, 5%, 10%, 15%, 20%, 25% and 30% MGL nanoparticles were incorporated into the polypropylene matrix and then the measurement of the conductivity was made by electrochemical impedance spectroscopy (EIS). From the theoretical point of view, we incorporate quantum effects to describe the percolation phenomenon. Quantum effects estimated using electronic structure calculations to describe the ion transport phenomenon are explored, and then these results are used in a conductivity approach and compared with the experimental values.

2. Methods

2.1 Sample preparation

Multilayer graphene (MLG) was purchased from XGScience. Grade *M* with a diameter of 5 μm was selected for the trials, which is claimed to have high thermal and electrical properties. Homopolymer polypropylene (PP) was selected for the polymer matrix. Polypropylene was selected because it has a non-polar behavior, and thus we can study the behavior of graphene nanoparticles in the polymer. The grade employed was PP DUCOR 1101S from DUCOR Petrochemicals. This material has an MFR (230 °C/2.16 kg) of 25 g/10 min, a tensile modulus of 1500 MPa, and a melting point of 163 °C.

Nanocomposites with different percentages of MLG (PP+%MLG) were obtained in a co-rotative twin screw extruder COPERION W&P ZSK25. The extruder has a diameter of 25 mm and an L/D ratio of 40. MLG nanocomposites were obtained with 0.5%, 1%, 3%, 5%, 10%, 15%, 20%, 25% and 30% filler loading. All the nanocomposites were produced with the same processing conditions. The fillers were incorporated *via* a masterbatch produced in a previous process where an MLG loading of 15% was produced under the following optimized conditions:[19] a highly dispersive screw configuration, 600 rpm and a temperature profile of 260 °C/220 °C/220 °C/210 °C/200 °C/190 °C. The masterbatch dilutions were processed with the same temperature profile with a screw speed of 800 rpm and using a highly dispersive screw. Samples were obtained by compression molding in a hot press (COLLIN model P200E) at 200 °C/15 bars over 15 min. Electron micrographs were obtained using a Jeol JEM-1010 high-resolution microscope (JEOL, Japan). Dispersion analysis was carried out on samples with 5% MLG. A concentration of nanoparticles higher than 5% caused the matrix to collapse, and it was not possible to analyze the homogeneity and the particle size. In the ESI,† Fig. S1–S3 show the SEM images for PP+5%MLG. From these figures, we can see that MLG flakes are aligned in the same direction, and there is no evidence of agglomeration. Fig. S2b and S3b (ESI†) shows a detailed MLG flake forming the MLG particles in the matrix of PP. Also, using the appropriate software, we calculated that the value of mean particle size was (12.5 ± 1.6) μm and the agglomerate density was (5.6 ± 0.5)%.

Samples with dimensions of (10 × 1 × 0.4) cm were used to obtain electrical conductivity using impedance spectroscopy electrochemical (ISE) studies where, for all the samples, the thickness was (400 ± 10) μm.[19]

2.2 Dielectric properties

The complex conductivity and permittivity of the compounds were measured by impedance spectroscopy at several temperatures within the 293 K (20 °C)–333 K (60 °C) range and frequency window $10^{-1} < f < 10^{7}$ Hz using a Novocontrol Broadband Dielectric Spectrometer (Hundsangen, Germany) integrated with an SR 830 lock-in amplifier with an Alpha dielectric interface. The experiments were performed with 100 mV amplitude. PP+%MLG samples of (400 ± 10) μm thickness were placed between two gold electrodes. During the conductivity measurements, the temperature was kept isothermal or changed stepwise within the entire temperature range controlled by a nitrogen jet (QUATRO from Novocontrol) with a temperature error of 0.1 K for every single sweep in frequency.

2.3 Computational method

To effectively describe the compounds proposed in this work, electronic structure calculations were used. The graphene layer was designed as a 6 × 6 supercell, with a C–C bond length of 1.42 Å. The graphene layer is embedded in the *x*–*y* plane. Meanwhile, the dimension of the supercell in the *z*-axis is large enough to neglect the effects between layers (30 Å). In order to relate the experimental data to the computational simulation, we used *N* slabs (*N* = 1, 5, and 10); a monomer with 1 slab represents 30% filler and the polypropylene with 10 slabs represents 1% filler. The initial distance between the polypropylene and the graphene sheet, at least between the hydrogen atoms, is 3 Å. The ground-state structure, adsorption energy and density of states (DOS) have been calculated with the Quantum-Espresso Computational Package,[25] using a plane-wave set and pseudopotentials. Density Functional Theory (DFT)[26] was used with the generalized gradient approximation (GGA) and the Perdew–Burke–Ernzerhof parameterization (PBE).[27] Kohn–Sham orbitals were expanded in a plane-wave basis-set up to a kinetic energy cutoff of 40 Ry. The convergence criterion for the self-consistent calculation was 10^{-6} Ry; the Brillouin-zone integrations were carried out with the Methfessel–Paxton smearing technique,[28] the smearing parameter was 0.05 Ry. The Monksort–Pack approach[29] was used to select the *k*-point mesh, with *Γ*-centered at 4 × 4 × 1. The pseudopotentials for C, H, and O were chosen from the quantum espresso website.[30] All the pseudopotentials used the Vanderbilt approach.[31] The adsorption energy (E_{ads}) has been calculated according to the formula

$$E_{ads} = E_{graphene+mol} - (E_{graphene} + E_{mol}). \quad (1)$$

E_{ads} is a measurement of the thermodynamic stability of the system. In eqn (1), $E_{graphene+mol}$ represents the total energy of the system formed by the molecule adsorbed into the graphene sheet, $E_{graphene}$ is the total energy of the graphene sheet, and E_{mol} is the energy of the polypropylene molecule in the gas phase. If $E_{ads} < 0$, the adsorption process is exothermic, otherwise it is endothermic.

3. Results

Electrochemical impedance spectroscopy (EIS) measurements were carried out for all the samples of PP+%MLG at different temperatures (20 °C to 60 °C) to obtain information on the conductivity of the sample. Data for the real part of the conductivity were analyzed in terms of the corresponding Bode diagrams, where variations of the conductivity with the frequency for all the composites of PP+%MLG at different graphene concentrations (% = 0.5, 1, 3, 5, 10, 15, 20, 25 and 30) are shown in Fig. 1. In this plot, we can see the double logarithmic plot of the conductivity in S cm^{-1} *versus* frequency in (Hz) at 50 °C of temperature. A similar behavior was observed for the other temperatures and practically the same values of conductivity were obtained for each one of the temperatures. A close inspection of this figure shows that the real part of the conductivity of the samples in the range of 20 to 30% MLG is constant for all frequencies within the range studied. Notice that in the region where the conductivity presents a plateau, the phase angle tends to zero, the imaginary part of the impedance will be zero, and then this value represents the dc-conductivity. This behavior typical of conductor materials.[32–35] However, the conductivity is a function of the number of fillers that we have incorporated in the nanocomposite. On the other hand, for the PP+15%MLG nanocomposite, we observe that the conductivity is practically constant over the whole range of frequencies, and only at frequencies higher than 10^6 Hz does the behavior of the sample show a cut-off frequency where it starts increasing with the frequency. In the samples whose behavior is not that of a pure conductor, in the regions of high frequencies, there is a decrease of the conductivity when frequency decreases. This can be explained as a Debye relaxation due to the macroscopic polarization of the charges as a consequence of the electric field applied. This relaxation is characterized by a relaxation time, which depends on the temperature, chemical structure of the samples and their thickness. This behavior may be due to the reorientation motion of dipoles and more likely to the motion of the localized charges, which dominate the dc-conductivity.[36–39]

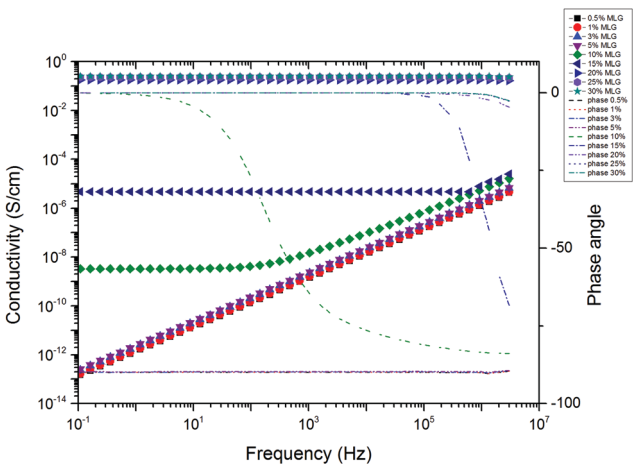

Fig. 1 Bode diagram for the samples of PP+MLG showing the conductivity and phase angle for all the samples at 50 °C.

Similar observations can be made for the sample of PP+10%MLG where the real part of the conductivity is also constant at the low frequency region until a cut-off frequency where it starts increasing with the frequency as if the sample were a capacitor. Finally, for the other samples with a lower content of graphene oxide, the plateau is not observed, presumably because it is at very low frequencies, outside the range of measurement for our experiments, showing a dielectric behavior for the samples. The value of σ being constant with the frequency means that the impedance has only a resistive contribution and its value represents the electrical conductivity of the sample. The value of the conductivity of each one of the nanocomposites can be obtained from the intercept in the OY-axis, (*i.e.* from the intersection of the extrapolated frequency-independent plateau line). Notice that in the case of the percentage of fillers being 15% or less, the tendency is to change the resistor to a capacitor behavior in the high frequencies region. The critical frequency is a function of the amount of MLG filler. For amounts of MLG below 10%, our results show straight lines with the slope *ca.* −1, indicating that the nanocomposite at these concentrations is purely a capacitor, where the values of the geometrical capacitance C, for the samples of low contents of MLG (% = 0.5, 1, 3, 5), will be dependent on the amount of MLG incorporated into the matrix of polypropylene. Fig. 1 shows that by increasing the number of MLG nanoparticles in the polypropylene film, the conductivity increases. The trend shows that by increasing the percentage of MLG nanoparticles over 15–20%, the electrical conductivity will have the characteristic behavior of pure graphene.[40]

Fig. 2 shows the relationship between the conductivity and the percentage of MLG nanoparticles added into the polypropylene matrix. The percolation threshold is around 18% MLG nanoparticle fillers. Fig. 2 was made using the experimental conductivity and then fitted with the Boltzmann Sigmoid, according to the equation:

$$y = \frac{-0.23521}{1 + e^{(x-18.204/1.03592)}} - 0.23521, \quad (2)$$

with an error fit of R^2 = 0.905. To accomplish a theoretical model of the conductivity of these nanocomposite materials, we need to perform a study of the interaction effects between the polypropylene matrix and the graphene.[41] Electronic structure calculations were carried out using a graphene supercell of 6 × 6 with adsorption of a polypropylene chain, which is formed with different slabs. Fig. 3 shows the ground-state structures of the computational simulation for graphene–polypropylene (N = 10, N = 5, and N = 1).

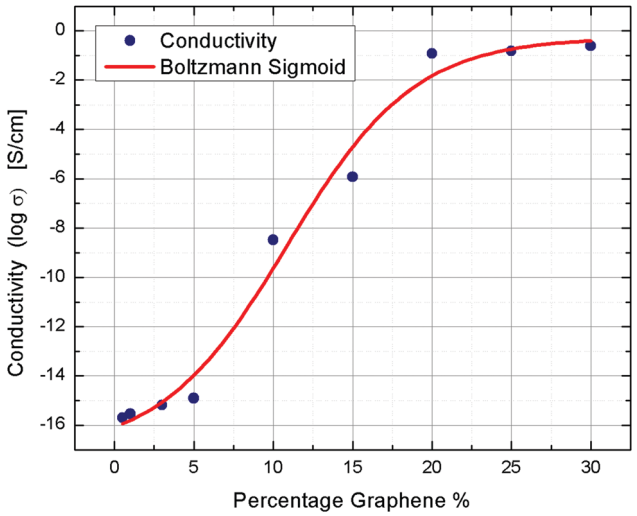

Fig. 2 The experimental electrical conductivity *versus* the percentage of MLG nanoparticles deposited in the polypropylene matrix.

Table 1 The distance between the polypropylene and the graphene sheet is called the bond length and these distances (Å) and the adsorption energies (eV//kcal mol^{-1}) are presented for the graphene–polypropylene with *N* slabs

N of graphene–polypropylene	Bond length (Å)	Adsorption energy (eV//kcal mol^{-1})	$\|\varepsilon - E_F\|$
N = 1	4.29 (2)//4.35	−0.057//−1.32	0.14
N = 5	4.28(6)//5.06 (5)	−1.81//−41.62	0.73
N = 10	4.29(7)//4.62 (9)//5.06 (5)	−3.77//−86.76	1.55

Table 2 Deformation parameters from the graphene–polypropylene systems (height *z* and radius *R*), the aspect ratio α, the S_{11} element of the Eshelby tensor, and c_1* in the percolation threshold for each system

N of graphene–polypropylene	*z* (Å)	*R* (Å)	α	S_{11}	c_1*	Percolation threshold (%)
1	0.26	4.01	0.064	0.472	0.171	17.1
5	0.47	6.35	0.074	0.468	0.183	18.3
10	0.349	4.62	0.054	0.476	0.185	18.5

From Fig. 3, it is possible to see the ground-state structure for the system graphene–polypropylene with three different slabs. The polypropylene carbons are shadowed in blue only for distinguishing them from the carbons of the graphene. The initial distance between the polypropylene axis and the graphene sheet (C–C) was 2.8 Å. However, after the geometry optimization, the polypropylene moves away from the surface. Table 1 shows the distance between the polypropylene axis and the graphene sheet, called the bond length, which is calculated from one central carbon atom of the polypropylene and another carbon atom of the graphene sheet (C–C). Also, it shows the adsorption energies of each system.

From the facts that the polypropylene moves away from the graphene sheet and that the adsorption energies are very small, in the physisorption range, the van der Waals forces are the only forces interacting between the polymer and the graphene. Of the optimized geometries, it can be observed that the polypropylene does not modify the graphene surface. Initially, the polypropylene film was chosen as the matrix for the deposition of MLG nanoparticles, because polypropylene films present a non-polar behavior and this was thought to avoid the influence of the film on the MLG nanoparticle. From the simulations, it was observed that this assumption is appropriate, since the polypropylene moves away from the surface of graphene, minimizing the interactions between the polymer matrix and the MLG nanoparticles. By comparing the bond lengths of the separated compounds before and after the adsorption, we see that these bond lengths remain unchanged after the adsorption phenomena occur. Because of the way in which the adsorption phenomenon happens (physisorption and bond lengths unchanged), we observe that there are two places where the

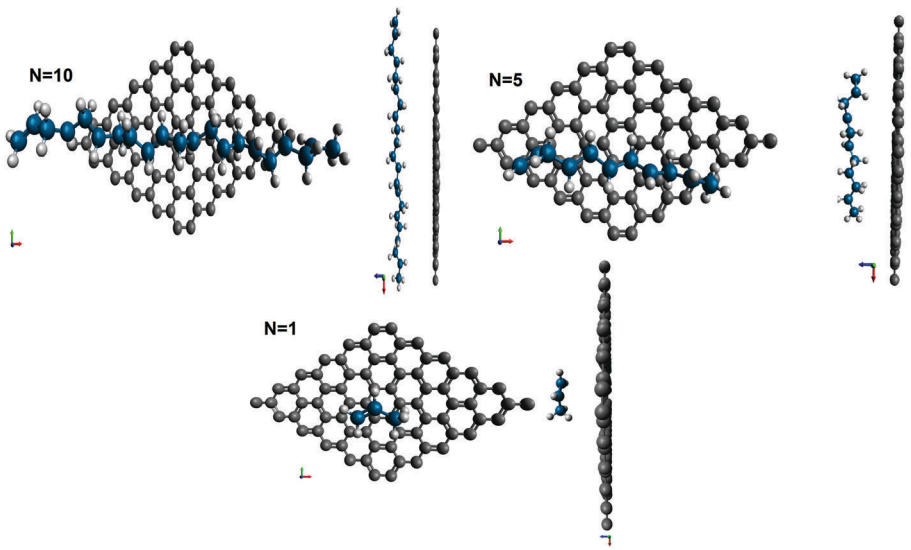

Fig. 3 Ground-state structures of polypropylene $(C_3H_6)_N$ (*N* = 10, 5, and 1), the value of *N* indicates the slabs; adsorption on a graphene supercell (6 × 6); the carbons of the polypropylene are shadowed in blue only for the purpose of distinguishing them from the carbons of the graphene sheet.

charge carriers are confined; in the p-bonds of the polypropylene and the π-bonds of the graphene sheets. We concluded that before the percolation threshold, the charge carriers are trapped in the p-bonds of the polypropylene, inhibiting the transport. Meanwhile, after the percolation threshold, the transport of the charge carriers is acquired through the π bonds formed by the graphene sheet, improving transport.

We observed that introducing the MLG nanoparticles into the polypropylene matrix enhanced the conductivity of the polymer, transforming the polypropylene sheet from an insulating to a conductive material. It is possible to see that filling of the MLG nanoparticles in the polypropylene occurs as a non-linear function of the filler concentration. In fact, the filler concentration follows a percolation threshold, which is influenced by several factors such as the aspect ratio of graphene sheets, inter-sheet junction, wrinkles, folds, *etc.*[42]

For the sake of describing the interaction between the polypropylene matrix and the graphene nanoparticles, it is important to characterize the interface effects. The interface effect is a result of the interfacial charge carrier tunneling, enhancing the interfacial conductivity, which depends on the filler percentage.[20,24] When the filler percentage increases, the average distance between fillers decreases, causing the extra charge carriers to move across the interface between the MLG nanoparticles and the polypropylene matrix. The electronic density of states (DOS) indicates how the charge carriers find a way to move.

The LDOS for pure graphene and graphene–polypropylene is shown in Fig. 4. The grey line represents the LDOS of pure graphene, and the blue/green/red line is the LDOS for a graphene–polypropylene system with N slabs (N = 1, 5, and 10). It is well known that in weakly disordered solids, which is the case according to the adsorption energies, the LDOS appears to be slightly different from the ideal case.[43] In those systems in which the MLG nanoparticles have a predominant effect, after the percolation threshold, the Fermi energy (E_F) of the graphene–polypropylene system (N = 1, and N = 5) is located to the right of the Dirac point, considering the Dirac point as the Fermi energy of pure graphene, remaining in the system as an n-type doped system. The charge transfer mechanism occurs from the polypropylene molecule to the graphene surface, because the localized states of the graphene–polypropylene system exceed the Dirac point,[44] stimulating the electronic transport. Before the percolation threshold (graphene–polypropylene N = 10 slabs), the LDOS tends to shift to the left of the LDOS of pure graphene, inhibiting the transport of the charge carriers. The E_F is on the left side of the Dirac point, indicating that the system is p-type doped. The charge transfers from the graphene sheet to the polypropylene.

We used classic descriptions of the conduction channels of the nanocomposite and incorporated quantum effects in the aspect ratio. In particular, we applied the theoretical description made by Weng *et al.*[45,46] They modeled the percolation phenomenon using the Eshelby's tensor.[47,48] The Eshelby's tensor is a fourth order tensor S_{ijkl}, which describes the inclusion of a finite volume over a homogeneous matrix material. If the inclusion has an ellipsoidal shape, the Eshelby's tensor is reduced to a tensor of the second order S_{ij}. In this work, the Eshelby's tensor is defined according to Landau and Lifshitz:[49]

$$S_{11} = S_{22} = \begin{cases} \dfrac{\alpha}{2(1-\alpha^2)^{\frac{3}{2}}}\left[\cos^{-1}\alpha - \alpha\left(1-\alpha^2\right)^{\frac{1}{2}}\right], & \alpha < 1; \\ \dfrac{\alpha}{2(\alpha^2-1)^{\frac{3}{2}}}\left[\alpha\left(\alpha^2-1\right)^{\frac{1}{2}} - \operatorname{arccosh}\alpha\right], & \alpha > 1; \end{cases}$$

$$S_{33} = 1 - 2S_{11}.$$

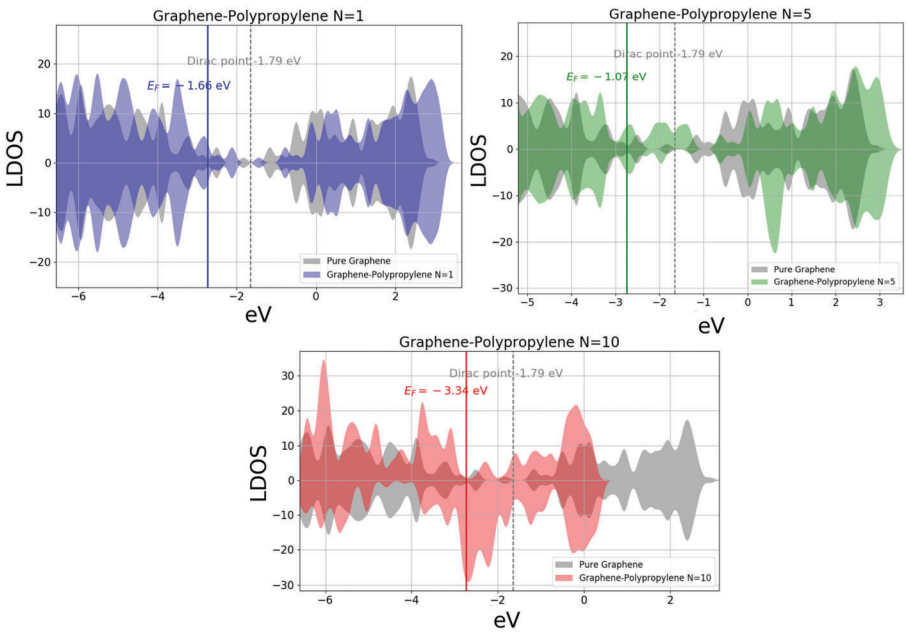

Fig. 4 The local electronic density of states (LDOS) for pure graphene and the graphene–polypropylene system.

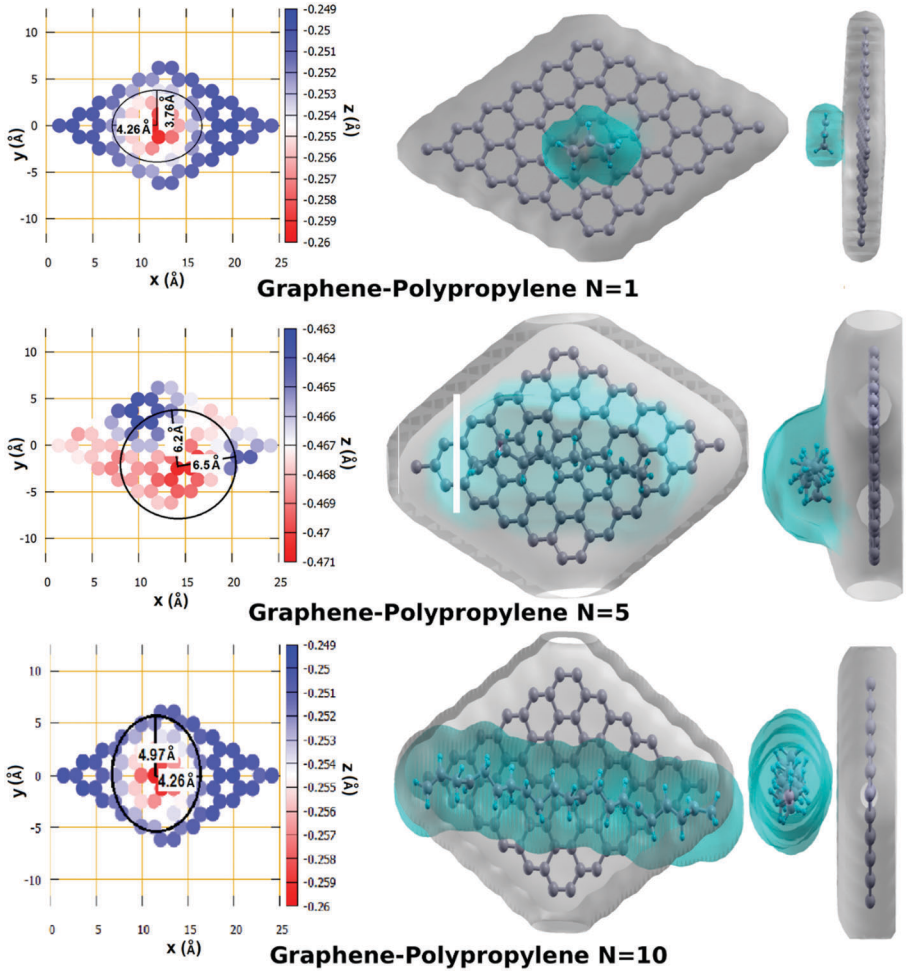

Fig. 5 The optimized geometry of graphene–polypropylene with N slabs (N = 1, 5, and 10) is shown. It shows the deformation of the graphene sheet produced by the polypropylene with the coordinates and with the Charge Density Surface (CDS).

This definition of the Eshelby's tensor used a geometrical parameter defined as the aspect ratio α, which is the thickness–diameter ratio of the fillers. With this definition of the Eshelby's tensor, it is possible to calculate (c_1*) in the percolation threshold with the expression for low frequencies:

$$c_1 = \frac{18S_{11}^3 - 9S_{11}}{18S_{11}^2 - 3S_{11} - 4}. \quad (3)$$

In previous studies,[50,51] the formation of propagation channels and tunneling from the Cauchy statistical function is considered, and the most common computational treatment for this system is using the Monte Carlo simulation. In this work, the quantum effects are considered in the electronic structure calculations and in the deformation measurement, as shown in Fig. 5. The coordinates of the carbon atoms of the graphene sheet were plotted to obtain the deformation parameters.[52] The heights of the graphene sheet (z) are taken as the fluctuation of the z-axis, considering that the graphene sheet, in the beginning, was placed in the plane z = 0. The heights are shown in a blue–red scale. The deformation radius was taken as the distance between the maximum and minimum height near the polypropylene molecule. Another way to obtain the deformation radius is using the charge density surface (CDS). The aspect ratio was defined as the ratio (α) between the height (z) and the deformation radius (R), $\alpha = \frac{z}{R}$.

In the percolation threshold, the conductivity behaves, predominantly, like graphene. The aspect ratio was defined as the ratio (α) between the height (l) and the deformation radius (R), $\alpha = \frac{l}{R} = 0.0468$, delivering a percolation threshold of 18.3% of the MLG nanoparticle. The experimental measurement of c_1* in the percolation threshold is around 18% of MLG nanoparticles.

Following previous studies about graphene conductivity,[52] the theoretical conductivity of graphene can be estimated in terms of the elastic deformation of the graphene sheet. In our case, a conductivity measurement was made of the polypropylene matrix. After the percolation threshold, the conductivity behaves similar to the conductivity of graphene doped with polypropylene. At this point, we are using the approach of Wehling *et al.*, which is:

$$\sigma \approx \left(\frac{4e^2}{\pi h}\right)\frac{n_e}{n_i}\ln^2\left|\frac{E_F}{D}\right|. \quad (4)$$

In this approach, we consider that the scattering mechanism is mid-gap states.[53] In Wehling *et al.'s* paper, they deduced this conductivity formula in terms of the Green's function in two dimensions. D is a parameter defined in terms of the nearest neighbor hopping (t), $D = \sqrt{\sqrt{3}\pi t}$, and according to Wehling's work, it is possible to calculate D in terms of the graphene deformation parameter, $D = hv_F/R$; R is the deformation radius. From the optimization of the geometry,[54] it is viable to estimate E_F of the graphene–polypropylene system and D as a function of $v_F = \sqrt{2E_F/m_e}$ ($m_e = 9.1 \times 10^{-31}$ kg is the mass of the electron); n_i is the number of impurities in 1 cm^2; n_e is the number of charge carriers in 1 cm^2, and n_e increases as the amount of MLG nanoparticles increases. The MLG nanoparticles are randomly deposited so at a minimum percentage of MLG (percolation threshold), charge carriers and at least one conductive channel in which the charge carriers would flow through the polymer matrix will be found. The conductive and insulating regions will be combined, so there will be a thermodynamic fluctuation between them, turning the insulation region into a conductive area.

The terms of eqn (4) are determined directly from the optimization of the geometry, except for the fraction n_e/n_i. The fraction n_e/n_i represents the fluctuation of charge carriers available in the system. When the system is insulated, there are no charge carriers available for transport in the material, but as soon as the MLG nanoparticles are deposited in the system, there is exponential growth. The growth of charge carriers available for transport is described by the following differential equation:

$$\frac{dy}{dx} = \alpha y\left(1 - \frac{y}{k}\right),$$

where we use $y = n_e/n_i$. The solution to this differential equation is given by the logistic equation $\frac{n_e}{n_i} = \frac{k}{1 + e^{d-\alpha x}}$. Again, following Weng *et al.'s* description,[45] the parameters of this logistic equation are given by the deformation of the system; k is the asymptote value, given by the point of inflexion $k = 24$; d is the percolation threshold; α is the aspect ratio defined below as a geometrical parameter obtained directly from the simulation ($\alpha = 0.049$).

In Table 3, the n_e/n_i parameters were calculated directly from the logistic equation. Then, these values were introduced into eqn (4) and compared with the experimental conductivity. It looks like the logistic equation is a good approach to describe the percolation problem with slight differences between the experimental and theoretical conductivity. The difference emerges before the percolation threshold, in which the composites behave like an insulator because our theoretical approach is designed for composites with graphene. Fig. 6 shows the direct comparison between the theoretical and the experimental sigmoid. The experimental sigmoid is calculated in Fig. 2 and obeys eqn (2). The theoretical one is fitted with the Boltzmann Sigmoid, according to the equation:

$$y = \frac{-0.23701}{1 + e^{(x-17.997/0.99808)}} - 0.23711,$$

with an error fit of $R^2 = 0.96845$.

Table 3 Estimation of the charge impurity ratio n_e/n, using the exponential growth model. Also, a direct comparison between the experimental conductivity and the theoretical conductivity is shown

%MLG	n_e/n_i	σ_{the} (S cm^{-1})	σ_{exp} (S cm^{-1})
0.5	0.00001	5.96×10^{-12}	2.1×10^{-16}
1	0.00002	9.82×10^{-12}	2.83×10^{-16}
3	0.00011	7.25×10^{-11}	6.5×10^{-16}
5	0.00049	5.36×10^{-10}	1.24×10^{-15}
10	0.02193	7.95×10^{-8}	3.39×10^{-9}
15	0.94947	0.0112	1.23×10^{-4}
20	17.6014	0.209	0.18
25	28.9656	0.237	0.225
30	29.3901	0.237	0.24

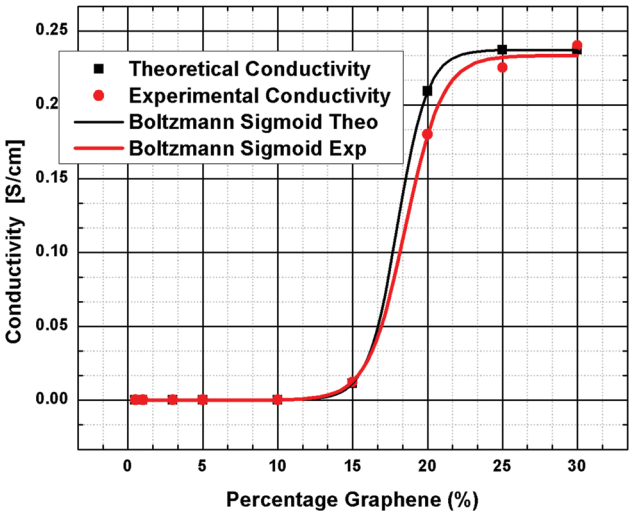

Fig. 6 The theoretical conductivity *versus* the percentage (%) of MLG nanoparticles deposited in the polypropylene matrix (black color) is shown. On the other hand, in red color, we show the experimental results for the same percentages of graphene. The lines show the sigmoid fits for both experimental and theoretical results.

4. Conclusions

We studied the compounds formed by graphene surfaces and polypropylene membranes. This study is divided into two parts; experimental and computational analysis. In both analyses, we observed that the conductivity curve could be fitted by a sigmoid curve, which is the main characteristic of the percolation phenomenon. The percolation threshold is around 18% MLG nanoparticles. Likewise, the theoretical description of the percolation is based on the quantum framework, leading to a more accurate description, very similar to the experimental results. The percolation threshold depends only on a geometrical parameter (the aspect ratio α), and we incorporated the quantum effects in this α, specifically in the optimization of the geometry. The consideration of these quantum effects in the percolation threshold gives a result very similar to the experimental threshold observed.

From the electronic structure, it can be seen that the interactions between graphene and the polypropylene are of the van der Waals type. From the DOS, we see that increasing the number of slabs in the polypropylene raises the energy gap, making the system insulated. This characteristic made it possible to determine that before the percolation threshold, the charge carriers are trapped in the p-bonds of the polypropylene, restricting the transport and the charge is transferred from the graphene sheet to the polypropylene (this mechanism is not so efficient, so the charge transport is very poor), causing p-type doping. After the percolation threshold, the charge carriers are transported through the π-bonds of the graphene sheet and the charge is transferred from the polypropylene to the graphene sheet causing n-type doping, improving the charge transport and turning the material into a conductive one.

The electrical conductivity was calculated using an approach with graphene; this approach considered the quantum conductance of graphene and the mid-gap state mechanism to describe the scattering of the charge carriers. As soon as the MLG nanoparticles are introduced into the system, an exponential growth of the number of charge carriers in the composite material appears. The percolation phenomenon was introduced in the conductivity approach as the n_e/n_i ratio (see eqn (4)). The theoretical conductivity estimate in this work is adequate compared to the experimental conductivity (see Table 2), considering the interface between the polypropylene and the MLG nanoparticles.

Conflicts of interest

There are no conflicts to declare.

Acknowledgements

This research has been supported by the ENE/2015-69203-R project, granted by the Ministerio de Economía y Competitividad (MINECO), Spain. Also, the authors are grateful to UNAM-DGAPA-PAPIIT projects IG 100618 y IG 114818, DGTIC-UNAM for access to the Miztli-UNAM supercomputer LANCAD-UNAM-DGTIC-055, and UNAM-DGAPA for the Postdoctoral grant for Roxana M. del Castillo.

References

1 H. G. Karian, *Handbook of polypropylene and polypropylene composites*, RheTec, Inc., Whitmore Lake, Michigan, 2nd edn, 2003, https://books.google.es/books?hl=es&lr=&id=C0nzeNPUpoIC&oi=fnd&pg=PP1&dq=Handbook+of+polypropylene+and+polypropylene+composites&ots=LYqYBYg45n&sig=3gtYXigr8_O8CUJeefBCtGI7QXA#v=onepage&q=Handbook%20of%20polypropylene%20and%20polypropylene%20composites&f=false.

2 T. Rath and Y. Li, Nanocomposites Based on Polystyrene-B-Poly (Ethylene-R-Butylene)-B-Polystyrene and Exfoliated Graphite Nanoplates: Effect of Nanoplatelet Loading on Morphology and Mechanical Properties, *Composites, Part A*, 2011, **42**(12), 1995–2002. http://www.sciencedirect.com/science/article/pii/S1359835X11002867.

3 M. S. Kim, J. Yan, K. M. Kang, K. H. Joo, Y. J. Kang and S. H. Ahn, Soundproofing Ability and Mechanical Properties of Polypropylene/Exfoliated Graphite Nanoplatelet/Carbon Nanotube (PP/xGnP/CNT) Composite, *Int. J. Precis. Eng. Man.*, 2013, **14**(6), 1087–1092, DOI: 10.1007/s12541-013-0146-3.

4 K. Zhang, H. O. Yu, Y. D. Shi, Y. F. Chen, J. B. Zeng, J. Guo, B. Wang, Z. Guo and M. Wang, Morphological regulation improved electrical conductivity and electromagnetic interference shielding in poly(L-lactide)/poly(ε-caprolactone)/carbon nanotube nanocomposites via constructing stereocomplex crystallites, *J. Mater. Chem. C*, 2017, **5**, 2807–2817. http://pubs.rsc.org/-/content/articlehtml/2017/tc/c7tc00389g.

5 P. Bhawal, T. K. Das, S. Ganguly, S. Mondal, R. Ravindren and N. C. Das, Fabrication of Light Weight Mechanically Robust Short Carbon Fiber/Ethylene Methyl Acrylate Polymeric Nanocomposite for Effective Electromagnetic Interference Shielding, *J. Polym. Sci. Appl.*, 2017, **1**(2), 1000107. https://www.scitechnol.com/peer-review/fabrication-of-light-weight-mechanically-robust-short-carbon-fiberethylene-methyl-acrylate-polymeric-nanocomposite-for-effective-e-QmFo.php?article_id=6532.

6 A. Masand, M. Borah, A. K. Pathak and S. R. Dhakate, Effect of filler content on the properties of expanded- graphite-based composite bipolar plates for application in polymer electrolyte membrane fuel cells, *Mater. Res. Express*, 2017, **4**(9), 095604, DOI: 10.1088/2053-1591/aa85a5/meta.

7 N. Afiqah, M. Radzuan, M. Y. Zakaria, A. Bakar Sulong and J. Sahari, The effect of milled carbon fibre filler on electrical conductivity in highly conductive polymer composites, *Composites, Part B*, 2017, **110**, 153–160. https://www.sciencedirect.com/science/article/pii/S1359836816307120.

8 Q. Li, F. Z. Yao, Y. Liu, G. Zhang, H. Wang and Q. Wang, High-Temperature Dielectric Materials for Electrical Energy Storage, *Annu. Rev. Mater. Res.*, 2018, **48**, 3.1–3.25, DOI: 10.1146/annurev-matsci-070317-124435.

9 Y. Qiaoa, X. Yina, T. Zhua, H. Lib and C. Tang, Dielectric polymers with novel chemistry, compositions and architectures, *Prog. Polym. Sci.*, 2018, **80**, 153–162.

10 A. Rosehr and G. A. Luinstra, Polypropylene composites with finely dispersed multi-walled carbon nanotubes covered with an aluminium oxide shell, *Polymer*, 2017, **120**, 164–175, http://www.sciencedirect.com/science/article/pii/S0032386117305220.

11 K. I. Bolotin, K. J. Sikes, Z. Jiang, M. Klima, G. Fudenberg, J. Hone, P. Kim and H. L. Stormer, Ultrahigh electron mobility in suspended graphene, *Solid State Commun.*, 2008, **146**, 9–10. http://www.sciencedirect.com/science/article/pii/S0038109808001178.

12 L. Banszerus, M. Schmitz, S. Engels, M. Goldsche, K. Watanabe, T. Taniguchi, B. Beschoten and C. Stampfer, Ballistic Transport Exceeding 28 μm in CVD Grown Graphene, *Nano Lett.*, 2016, **16**(2), 1387–1391, DOI: 10.1021/acs.nanolett.5b04840.

13 B. Terrés, L. A. Chizhova, F. Libisch, J. Peiro, D. Jörger, S. Engels, A. Girschik, K. Watanabe, T. Taniguchi, S. V. Rotkin,

J. Burgdörfer and C. Stampfer, Size quantization of Dirac fermions in graphene constrictions, *Nat. Commun.*, 2016, **7**, 11528. https://www.ncbi.nlm.nih.gov/pmc/articles/PMC4876454/.

14 S. Ansari and E. P. Giannelis, Functionalized graphene sheet poly(vinylidene fluoride) conductive nanocomposites, *J. Polym. Sci., Part B: Polym. Phys.*, 2009, **47**(9), 888–897, DOI: 10.1002/polb.21695/full.

15 H. B. Zhang, W. B. Zheng, Q. Yan, Y. Yang, J. W. Wang, Z. H. Lu, G. Y. Ji and Z. Z. Yu, Electrically conductive polyethylene terephthalate/graphene nanocomposites prepared by melt compounding, *Polymer*, 2010, **51**(5), 1191–1196. http://www.sciencedirect.com/science/article/pii/S003238611000056X.

16 D. D. L. Chung, A review of exfoliated graphite, *J. Mater. Sci.*, 2016, **51**(1), 554–568, DOI: 10.1007/s10853-015-9284-6.

17 T. Bayerl, A. Benedito, A. Gallegos, G. B. Mitschang and B. Galindo, Melting of Polymer-Polymer Composites by Particulate Heating Promoters and Electromagnetic Radiation, in *Synthetic Polymer-Polymer Composites*, ed. D. Bhattacharyya and S. Fakirov, Carl HanserVerlag GmbH & Co. KG, 2012, ch. 24, pp. 39–64, DOI: 10.3139/9781569905258.002.

18 J. Harper, D. Price and J. Zhang, Use of Fillers to Enable the Microwave Processing of Polyethylene, *J. Microwave Power Electromagn. Energy*, 2007, 219–227, DOI: 10.1080/08327823.2005.11688543.

19 B. Galindo, A. Benedito, E. Gimenez and V. Compañ, Comparative study between the microwave heating efficiency of carbon nanotubes *versus* multilayer graphene in polypropylene nanocomposites, *Composites, Part B*, 2016, **98**, 330–338. http://www.sciencedirect.com/science/article/pii/S1359836816305698.

20 M. Terrones, O. Martín, M. González, J. Pozuelo, B. Serrano, J. C. Cabanelas, S. M. Vega-Díaz and J. Baselga, Interphases in Graphene Polymer-based Nanocomposites: Achievements and Challenges, *Adv. Mater.*, 2011, **23**(44), 5302–5310, DOI: 10.1002/adma.201102036/full.

21 K. Asadi, A. J. Kronemeijer, T. Cramer, L. J. A. Koster, P. W. M. Blom and D. M. de Leeuw, Polaron hopping mediated by nuclear tunneling in semiconducting polymer at high carrier density, *Nat. Commun.*, 2013, **4**, 1710. https://search.proquest.com/docview/1349834005?pq-origsite=gscholar.

22 Z. Fan, F. Gong, S. T. Nguyen and H. M. Duong, Advanced multifunctional graphene aerogel-Poly(methyl methacrylate) composites: Experiments and modeling, *Carbon*, 2015, **81**, 396–404. http://www.sciencedirect.com/science/article/pii/S0008622314009245.

23 Z. Zabihi and H. Araghi, Monte Carlo simulations of effective electrical conductivity of graphene/poly(methyl methacrylate) nanocomposite: Landauer–Buttiker approach, *Synth. Met.*, 2016, **217**, 87–93. http://www.sciencedirect.com/science/article/pii/S037967791630073X.

24 X. Xia, Z. Zhong and G. J. Weng, Maxwell–Wagner–Sillars mechanism in the frequency dependence of electrical conductivity and dielectric permittivity of graphene–polymer nanocomposites, *Mech. Mater.*, 2017, **109**, 42–50. http://www.sciencedirect.com/science/article/pii/S0167663617300406.

25 P. Giannozzi, S. Baroni, N. Bonini, M. Calandra, R. Car, C. Cavazzoni, D. Ceresoli, G. Chiarotti and M. Cococcioni, *et al.*, QUANTUM ESPRESSO: a modular and open-source software project for quantum simulations of materials, *J. Phys.: Condens. Matter*, 2009, **21**(9), 395502, DOI: 10.1088/0953-8984/21/39/395502/meta.

26 F. M. Bickelhaupt and E. J. Baerends, Kohn–Sham Density Functional Theory: Predicting and Understanding Chemistry. in *Reviews in Computational Chemistry*, 2007, ed. K. B. Lipkowitz and B. Boyd Donald, John Wiley & Sons, Inc., vol. 15, pp. 1–89, DOI: 10.1002/9780470125922.ch1/summary.

27 J. P. Perdew, K. Burke and M. Ernzerhof, Generalized Gradient Approximation Made Simple, *Phys. Rev. Lett.*, 1996, **77**, 3865, DOI: 10.1103/PhysRevLett.77.3865.

28 M. Methfessel and A. T. Paxton, High-precision sampling for Brillouin-zone integration in metals, *Phys. Rev. B: Condens. Matter Mater. Phys.*, 1989, **40**, 3616, DOI: 10.1103/PhysRevB.40.3616.

29 H. J. Monkhorst and J. D. Pack, Special points for Brillouin-zone integrations, *Phys. Rev. B: Solid State*, 1976, 13, DOI: 10.1103/PhysRevB.13.5188.

30 Files: C.pbe-van_ak.UPF, H.pbe-van_ak.UPF, N.pbe-van_ak.UPF, and O.pbe-van_ak.UPF, http://www.quantum-espresso.org.

31 D. Vanderbilt, Soft self-consistent pseudopotentials in a generalized eigenvalue formalism, *Phys. Rev. B: Condens. Matter Mater. Phys.*, 1990, **41**, 7892, DOI: 10.1103/PhysRevB.41.7892.

32 T. S. Sorensen and V. Compañ, Complex permittivity of a conducting, dielectric layer containing arbitrary binary Nernst–Planck electrolytes with applications to polymer films and cellulose acetate membranes, *J. Chem. Soc., Faraday Trans.*, 1995, **91**(23), 4235–4250.

33 M. Drüschler, B. Hubber, S. Passerini and B. Roling, On Capacitive Processes at the Interface between 1-Ethyl-3-methylimidazolium tris(pentafluoroethyl)trifluorophosphate and Au(111), *J. Phys. Chem. C*, 2011, **115**, 6802–6808.

34 A. Serguei, M. Tress, J. R. Sangoro and F. Kremer, Electrode polarization and charge transport at solid interfaces, *Phys. Rev. B: Condens. Matter Mater. Phys.*, 2009, **80**, 184301.

35 F. Kremer and A. Schoenhals, *Broadban Dielectric Spectroscopy*, Springer, Berlin, 2003.

36 R. Coelho, Sur la relaxation d'une charge d'espace, *Rev. Phys. Appl.*, 1983, **18**, 137.

37 J. R. MacDonald, Theory of ac Space-Charge Polarization Effects in Photoconductors, Semiconductors, and Electrolytes, *Phys. Rev.*, 1953, **92**, 4.

38 J. Klein, S. Zhang, S. Dou, B. H. Jones, R. Colby and J. Runt, Modeling electrode polarization in dielectric spectroscopy: Ion mobility and mobile ion concentration of single-ion polymer electrolytes, *J. Chem. Phys.*, 2006, **124**, 144903.

39 B. M. Greenhoe, M. K. Hassan, J. S. Wiggins and K. A. Mauritz, Universal power law behavior of the AC conductivity versus frequency of agglomerate morphologies in conductive carbon nanotube-reinforced epoxy networks, *J. Polym. Sci., Part B: Polym. Phys.*, 2016, **54**(19), 1918–1923.

40 K. S. Novoselov, A. K. Geim, S. V. Morozov, D. Jiang, Y. Zhang, S. V. Dubonos, I. V. Grigorieva and A. A. Firsov, Electric Field Effect in Atomically Thin Carbon Films, *Science*, 2004, **306**(5696), 666–669. http://science.sciencemag.org/content/306/5696/666.

41 R. M. Del Castillo and L. E. Sansores, Study of the electronic structure of Ag, Au, Pt and Pd clusters adsorption on graphene and their effect on conductivity, *Eur. Phys. J. B*, 2015, **88**(248), 1–14, DOI: 10.1140/epjb/e2015-60001-2.

42 D. Galpaya, M. Wang, M. Liu, N. Mottam, E. Waclawik and C. Yan, Recent Advances in Fabrication and Characterization of Graphene-Polymer Nanocomposites, *Graphene*, 2012, **1**(2), 30–49. http://www.scirp.org/journal/PaperInformation.aspx?PaperID=23970.

43 I. Zvyagin. Charge Transport via Delocalized States in Disordered Materials. in *Charge Transport in Disordered Solids with Applications in Electronics*, ed. S. Baranovsky, John Wiley & Sons, Inc., 2006, pp. 1–48, DOI: 10.1002/0470095067.ch1/summary.

44 O. Leenaerts, B. Partoens and F. M. Peeters, Adsorption of small molecules on graphene, *Microelectron. J.*, 2009, **40**(4–5), 860–862. http://www.sciencedirect.com/science/article/pii/S0026269208005582.

45 R. Hashemi and G. J. Weng, A theoretical treatment of graphene nanocomposites with percolation threshold, tunneling-assisted conductivity and microcapacitor effect in AC and DC electrical settings, *Carbon*, 2016, **96**, 474–490. http://www.sciencedirect.com/science/article/pii/S0008622315303213.

46 X. Xia, Y. Wang, Z. Zhong and G. J. Weng, A frequency-dependent theory of electrical conductivity and dielectric permittivity for graphene–polymer nanocomposite, *Carbon*, 2017, **111**, 221–230. http://www.sciencedirect.com/science/article/pii/S0008622316308387.

47 J. D. Eshelby, The determination of the elastic fiel of an ellipsoidal inclusion, and related problems, *Proc. R. Soc. London, Ser. A*, 1957, **241**, 376–396. http://rspa.royalsocietypublishing.org/content/241/1226/376.

48 S. Trotta, F. Marmo and L. Rosati, Evaluation of the Eshelby tensor for polygonal inclusions, *Composites, Part B*, 2017, **115**, 170–181. http://www.sciencedirect.com/science/article/pii/S1359836816322132.

49 L. D. Landau, E. M. Lifshitz and L. P. Pitaevskii, *Electrodynamics of Continuous Media*, Pergamon Press, New York, 3rd edn, 1984.

50 Y. Wang, G. J. Weng, S. A. Meguid and A. M. Hamouda, A continuum model with a percolation threshold and tunneling-assisted interfacial conductivity for carbon nanotube-based nanocomposites, *J. Appl. Phys.*, 2014, **115**, 193706, DOI: 10.1063/1.4878195.

51 Y. Wang, J. W. Shan and G. J. Weng, Percolation threshold and electrical conductivity of graphene-based nanocomposites with filler agglomeration and interfacial tunneling, *J. Appl. Phys.*, 2015, **118**, 065101, DOI: 10.1063/1.4928293.

52 T. O. Wehling, S. Yuan, A. I. Lichtenstein, A. K. Geim and M. I. Katsnelson, Resonant Scattering by Realistic Impurities in Graphene, *Phys. Rev. Lett.*, 2010, **105**, 056802, DOI: 10.1103/PhysRevLett.105.056802.

53 T. Stauber, N. M. R. Peres and F. Guinea, Electronic transport in graphene: A semiclassical, *Phys. Rev. B: Condens. Matter Mater. Phys.*, 2007, **76**, 205423, DOI: 10.1103/PhysRevB.76.205423.

54 R. M. Del Castillo and L. E. Sansores. Adsorption of Metal Clusters on Graphene and Their Effect on the Electrical Conductivity, in *Graphene Materials – Advanced Applications*, ed. G. Z. Kyzas and A. C. Mitropoulos, INTECH, 2017, https://www.intechopen.com/books/graphene-materials-advanced-applications/adsorption-of-metal-clusters-on-graphene-and-their-effect-on-the-electrical-conductivity.